Available online at www.sciencedirect.com

ScienceDirect

Geochimica et Cosmochimica Acta 208 (2017) 24–40

Geochimica et Cosmochimica Acta

www.elsevier.com/locate/gca

Resetting of Mg isotopes between calcite and dolomite during burial metamorphism: Outlook of Mg isotopes as geothermometer and seawater proxy

Zhongya Hu [a], Wenxuan Hu [a,b,*], Xiaomin Wang [a], Yizhou Lu [a], Lichao Wang [c], Zhiwei Liao [d], Weiqiang Li [a,*]

[a] *State Key Laboratory for Mineral Deposits Research, School of Earth Sciences and Engineering, Nanjing University, Nanjing, Jiangsu 210093, PR China*

[b] *Institute of Energy Sciences, Nanjing University, Nanjing, Jiangsu 210093, PR China*

[c] *State Key Laboratory of Oil and Gas Reservoir Geology and Exploitation, School of Geoscience and Technology, Southwest Petroleum University, Chengdu, Sichuan 610500, PR China*

[d] *College of Resources and Environmental Science, Chongqing University, Chongqing 400044, PR China*

Received 15 November 2016; accepted in revised form 21 March 2017; available online 28 March 2017

Abstract

Magnesium isotopes are an emerging tool to study the geological processes recorded in carbonates. Calcite, due to its ubiquitous occurrence and the large Mg isotope fractionation associated with the mineral, has attracted great interests in applications of Mg isotope geochemistry. However, the fidelity of Mg isotopes in geological records of carbonate minerals (e.g., calcite and dolomite) against burial metamorphism remains poorly constrained. Here we report our investigation on the Mg isotope systematics of a dolomitized Middle Triassic Geshan carbonate section in eastern China. Magnesium isotope analysis was complemented by analyses of Sr-C-O isotopic compositions, major and trace element concentrations, and petrographic and mineralogical features. Multiple lines of evidence consistently indicated that post-depositional diagenesis of carbonate minerals occurred to the carbonate rocks. Magnesium isotope compositions of the carbonate rocks closely follow a mixing trend between a high δ^{26}Mg dolomite end member and a low δ^{26}Mg calcite end member, irrespective of sample positions in the section and calcite/dolomite ratio in the samples. By fitting the measured Mg isotope data using a two-end member mixing model, an inter-mineral $\Delta^{26}Mg_{dolomite\text{-}calcite}$ fractionation of 0.72‰ was obtained. Based on the experimentally derived Mg isotope fractionation factors for dolomite and calcite, a temperature of 150–190 °C was calculated to correspond to the 0.72‰ $\Delta^{26}Mg_{dolomite\text{-}calcite}$ fractionation. Such temperature range matches with the burial-thermal history of the local strata, making a successful case of Mg isotope geothermometry. Our results indicate that both calcite and dolomite had been re-equilibrated during burial metamorphism, and based on isotope mass balance of Mg, the system was buffered by dolomite in the section. Therefore, burial metamorphism may reset Mg isotope signature of calcite, and Mg isotope compositions in calcite should be dealt with caution in studies of carbonate rocks with thermal history. By contrast, Mg isotopes of dolomite are less prone to post-depositional resetting due to a number of properties including high Mg abundance and high thermodynamic stability, and Mg isotopes in dolomite may be a more robust recorder for original carbonate precipitates.
© 2017 Elsevier Ltd. All rights reserved.

Keywords: Magnesium isotope; Dolomite; Mixing; Burial metamorphism; Resetting

* Corresponding authors at: School of Earth Science and Engineering, Nanjing University, 163 Xianlin Avenue, Nanjing 210093, PR China.
E-mail addresses: huwx@nju.edu.cn (W. Hu), liweiqiang@nju.edu.cn (W. Li).

http://dx.doi.org/10.1016/j.gca.2017.03.026
0016-7037/© 2017 Elsevier Ltd. All rights reserved.

1. INTRODUCTION

Carbonate is ubiquitous on Earth, and its element and C–O–Sr isotope compositions have been extensively used to study paleo-environments (Cao et al., 2008; Song et al., 2015), dolomitization (Ronchi et al., 2011; Haas et al., 2014) and diagenetic processes (Mathieu et al., 2015; Kolchugin et al., 2016). Magnesium is an important component in most carbonate rocks, and advances in multi-collector inductively coupled plasma mass spectrometry (MC-ICP-MS) since 2000s have enabled high precision Mg isotope analyses, which led to an explosion of studies on Mg isotope geochemistry of carbonates (e.g., Galy et al., 2002; Young and Galy, 2004; Saenger and Wang, 2014; Teng, 2017; Teng et al., 2017).

A large variation in Mg isotope compositions has been discerned from terrestrial samples, particularly natural carbonates. In contrast to igneous rocks that have very limited Mg isotopic variability due to the lack of significant Mg isotope fractionation during fractional crystallization processes (Teng et al., 2010), natural carbonates, including aragonite, calcite, dolomite and magnesite, have remarkably low and variable δ^{26}Mg values, which range from ca. −1‰ to −5‰ (Saenger and Wang, 2014; Teng et al., 2017). Almost all carbonates of modern marine origin have δ^{26}Mg values that are lower than that of seawater ($\delta^{26}Mg_{seawater} \approx -0.8$‰; Ling et al., 2011). Broadly speaking, mineralogy is the first order control of Mg isotope compositions in carbonates, that the lowest δ^{26}Mg values in nature are reported from low Mg-calcite, which mainly range between −3‰ and −5‰ (Buhl et al., 2007; Pogge von Strandmann, 2008; Hippler et al., 2009; Immenhauser et al., 2010; Wombacher et al., 2011; Pogge von Strandmann et al., 2014), δ^{26}Mg values of high Mg-calcite, dolomite, aragonite and magnesite are progressively higher (Chang et al., 2004; Hippler et al., 2009; Wombacher et al., 2011; Geske et al., 2012, 2015a, 2015b; Lavoie et al., 2014; Dong et al., 2016). Experiments show that Mg isotope fractionations in Mg-calcite and aragonite are temperature dependent (Li et al., 2012; Wang et al., 2013), although the sensitivity of Mg isotope fractionation is small (0.01–0.02 ‰/°C). On the other hand, significant kinetic isotope effects during precipitation of calcite have been suggested in studies of Immenhauser et al. (2010) and Mavromatis et al. (2013). In addition, "vital effect", or processes related to biological activities have been found to affect Mg isotope fractionations in biogenic carbonates, as Mg isotope compositions of skeletons of marine animals are species-dependent (Hippler et al., 2009; Wombacher et al., 2011), although the exact mechanism of "vital effect" on Mg isotopes remains elusive.

Despite the complexities in fractionation behaviors, the large Mg isotope fractionation associated with carbonates has made Mg isotope a promising tool for studying the various geological processes recorded in carbonates, such as hydro-geochemical processes in a karst system (Riechelmann et al., 2012), hydrothermal fluid activities (Walter et al., 2015), precipitation of "molar tooth" carbonates in Precambrian oceans (Shen et al., 2016), as well as deglaciation events after the Snow Ball Earth event (Kasemann et al., 2014; Liu et al., 2014). On the other hand, Mg isotope composition of seawater is controlled by mass balance between Mg sources and sinks (Tipper et al., 2006), and in light of this, Mg isotope compositions of marine carbonates have attracted considerable interests for reconstruction of seawater δ^{26}Mg values in geological history because of their links to Mg cycling and global change. For example, Pogge von Strandmann et al. (2014) and Higgins and Schrag (2015) measured δ^{26}Mg values of low Mg-calcites in pelagic carbonates to reconstruct global Mg cycling in the Cenozoic, but considerable inconsistency exists between the two studies. Alternatively, Li et al. (2015) proposed that Mg isotopes in massive dolomite may be used to reconstruct Mg isotope compositions of ancient seawater.

In studies of carbonate sedimentary records using Mg isotopes, one of the challenges is to discern primary sedimentary signatures that reflect water chemistry from secondary post-depositional processes including early diagenesis, deep metamorphism and hydrothermal alteration. Overprinting and resetting of original isotopic signatures in carbonates have been widely documented for Sr, C and O isotope systems (Allan and Matthews, 1982; Elderfield and Gieskes, 1982; Banner, 1995). It is conceivable that Mg isotopes in carbonates are also subjective to post-depositional resetting, particularly for low Mg calcite and aragonite. Early diagenesis with continuous Mg supply from modified seawater via diffusion has been suggested to cause changes in Mg isotope compositions of carbonate sediments, and these changes could be constrained using reactive-transport models (Higgins and Schrag, 2010; Huang et al., 2015; Peng et al., 2016). The influences of diagenesis and burial metamorphism on dolomite rocks have been documented by Fantle and Higgins (2014) and Geske et al. (2012). The impact of diagenetic alteration on Mg isotope compositions of biogenic low-Mg calcite in brachiopod shell has been studied by Rollion-Bard et al. (2016) and Riechelmann et al. (2016) in detail. Despite these progresses, however, fundamental questions about the fidelity of Mg isotopes in carbonate rocks as recorders of primary seawater signatures remain unsolved. These questions include: (1) in carbonate rocks that contain both calcite and dolomite, do Mg isotopes in the two minerals respond differently to burial metamorphism? (2) is there a "closure temperature" for Mg isotopes in carbonates, that one can ignore post-depositional processes if the thermal history of the sample was below that temperature? (3) is there any isotopic signature that one can rely on to discriminate samples that have been reset in terms of the Mg isotopic system?

In this contribution, we studied the Mg isotope variability within a Middle Triassic carbonate section from Southeast China. The section has experienced a burial history that is well-documented, and the samples in the section contain carbonates with variable proportions of calcite and dolomite, these features make the section an ideal natural laboratory for investigation of the behavior of Mg isotopes in calcite during dolomitization and burial diagenesis. Our results reveal that Mg isotopes in carbonates can be reset at temperature as low as ca. 150 °C, therefore, caution is

urged in studies using Mg isotopes in calcite to refer primary sedimentological signatures; in contrast, Mg isotopes in dolomite seem to be more robust against post-depositional alteration.

2. GEOLOGICAL BACKGROUNDS AND SAMPLES

The study area is located at Geshan, Yixing City, in Lower Yangtze Block of Southeast China (Fig. 1A). The Lower Yangtze Block experienced two different sedimentological stages, including a marginal sea stage in the early Paleozoic, and an epicontinental sea stage in the Late Paleozoic-Early Mesozoic periods, when thick bedded carbonates were deposited (He et al., 2014). During the Middle Triassic, the Yangtze Plate drifted toward the North China Craton, closing up the ocean basin (Shu et al., 2004). In response, seawater depth in the Lower Yangtze Region gradually decreased and regional sedimentary system was dominated by restricted carbonate platform (Tong and Yin, 1997).

Excellent outcrops of Zhoucunchong Formation, early Anisian of Middle Triassic (~247 Ma) in age, are exposed as quarry mining sites at Geshan (Fig. 1A). Locally, the Zhoucunchong Formation is about 150 m in thickness and consists of carbonates ranging from limestone to dolostone, and interbeded gypsiferous rock (Jin, 2006). From bottom to top, gypsum contents and thickness of individual carbonate layer increase, and gypsum and dolomite become the dominant components of the upper Zhoucunchong Formation (Fig. 1B). Carbonates in the lower Zhoucunchong Formation are variably dolomitized, where limestone, dolomitic limestone, limy dolostone, and dolomstone layers co-exist and interbed each other without hiatus (Figs. 1C and 2). The regional strata subsided steadily until the end of Triassic. After middle Jurassic, the strata experienced several subsidence-uplift cycles, and reached its maximum burial depth (exceeding 3500 m) in the late Cretaceous (Hua, 2014; Huang et al., 2014). From the end of Cretaceous to the present, the regional strata have undergone continuous tectonic uplift caused by the Himalayan movement (Hua, 2014; Huang et al., 2014).

High density sampling of the Zhoucunchong Formation outcrop was performed at a quarry in 2013. The carbonates were sampled from a newly opened rock surface of the quarry (Fig. 3A and B; Appendix Fig. S1). The sampled rocks are fresh and devoid of any sign of surface weathering. Based on detailed field observation, the stratigraphic column of the lower Zhoucunchong Formation was divided

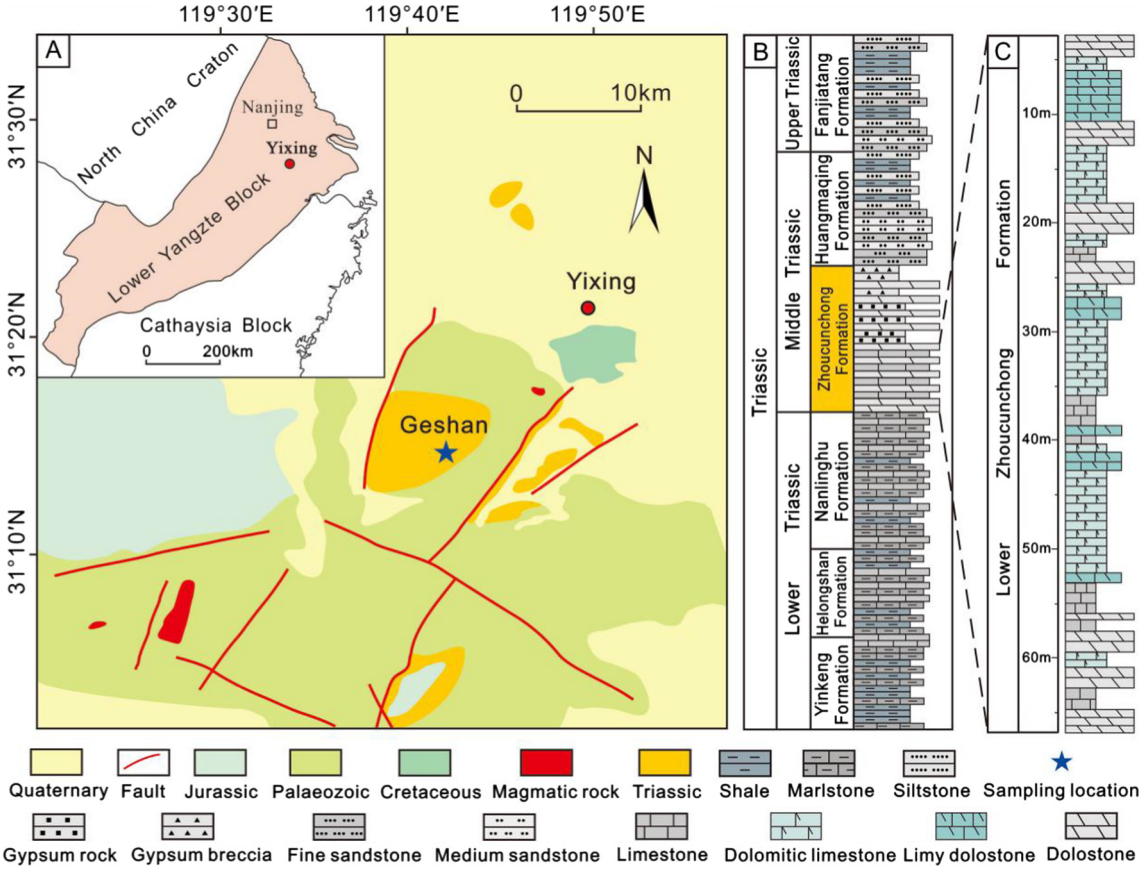

Fig. 1. Geological map showing sampling site and the Triassic stratigraphy of the Lower Yangtze Block. (A) Map showing the section and outcrop (modified from Wang et al., 2014); (B) stratigraphic column of Triassic in Lower Yangtze Block (modified from Tong and Yin, 1997); (C) detailed stratigraphy of the Lower Zhoucunchong Formation in Geshan section, based on field measurement.

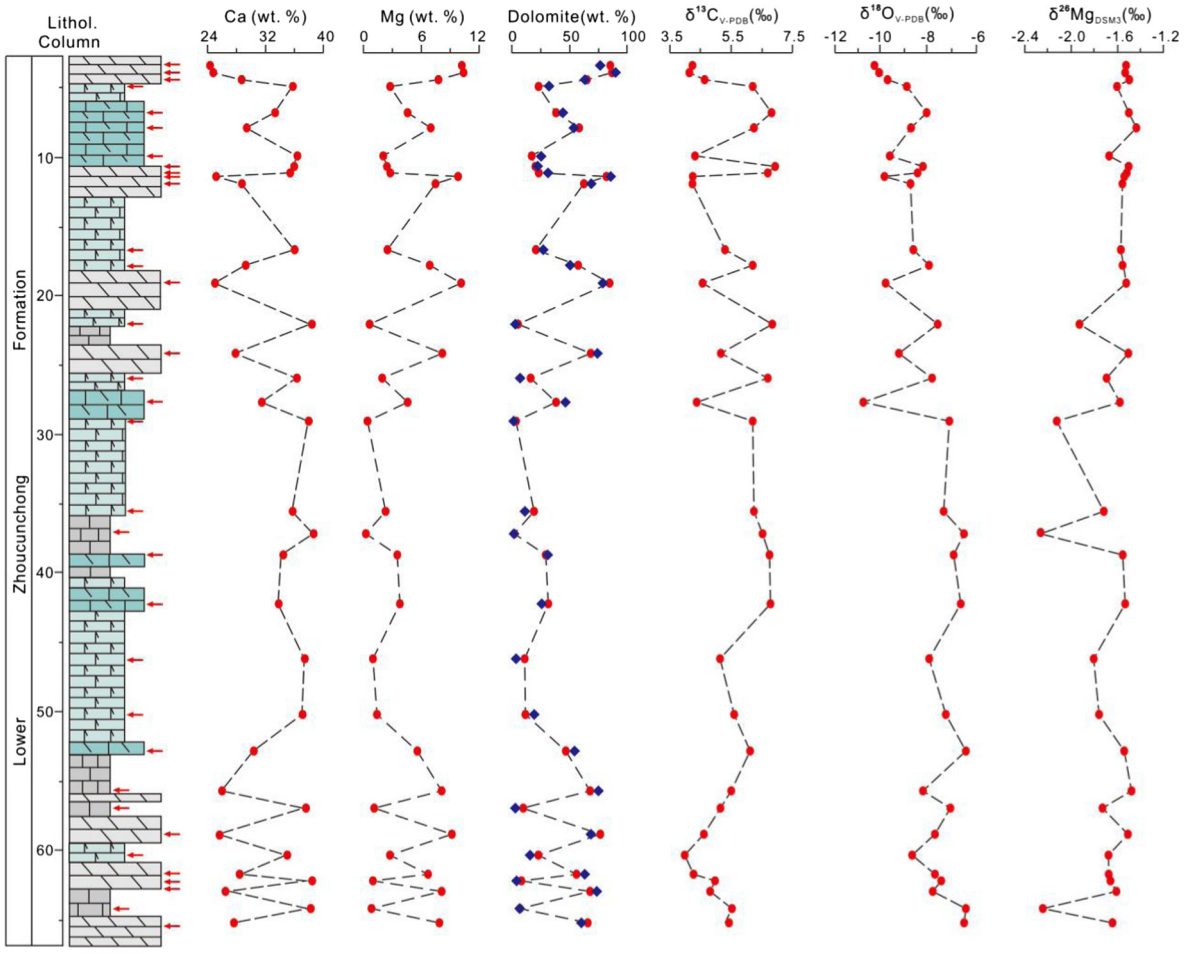

Fig. 2. Variation of lithology, major elements, mineral contents and stable isotope compositions of the Lower Zhoucunchong Formation. Red arrows mark the sample position along the stratigraphic column, the abundances of dolomite in each sample are calculated based on both bulk rock chemistry data (red circles) and powder XRD data (blue diamonds) respectively, Appendix Table S4 in detail. (For interpretation of the references to color in this figure legend, the reader is referred to the web version of this article.)

into 27 apparent layers over a true thickness of 68 m, where 35 representative samples were collected for this study (Fig. 2).

3. METHODS

3.1. Petrography and crystallography analyses

For petrographic characterization, one-half of each carbonate thin-section was stained by Alizarin Red-S and Potassium Ferricyanide to enhance the contrast between dolomite and calcite under microscope (Dickson, 1966). The other half was used for cathodoluminescence microscopy and backscatter electron microscopy. Cathodoluminescence microscopy was performed on a cold-cathode instrument (type CL8200-MK5) at Nanjing Institute of Geology and Palaeontology, Chinese Academy of Sciences with acceleration voltage of 12 kV, a current of 200–300 mA, and a chamber pressure of 0.03–0.05 mBar. Back scattered electron images were taken using a Hitachi SU1510 Scanning Electron Microscope at School of Earth Sciences and Engineering, Nanjing University.

Powder X-ray diffraction analysis of bulk sample powders was performed on a Rigaku Rapid II dual-source X-ray Diffractometer, using a rotating anode Cu target X-ray source (Cu $K\alpha = 1.5405$ Å) running at 40 kV and 100 mA. The instrument is equipped with an imaging plate, and 10 min exposure was used for each sample. Data processing and mineral identification were performed using a PDXL software. d values and intensities of (104) peaks for calcite and dolomite were obtained from the XRD spectrum using a PDXL software. The relative abundance of dolomite and calcite in bulk rocks was estimated from the intensities of the (104) peaks (Zevin, 1977). The Mg contents (or stoichiometry) of calcite and dolomite were calculated using the empirical curve by Zhang et al. (2010), who quantified the relationship between d_{104} value and the mole percent of $MgCO_3$ in the dolomite-calcite series. The degree of order of dolomite was calculated using the following equation by Graf and Goldsmith (1956):

$$R = I(015)/I(110)$$

where by I is the intensity of the peaks (015) and (110) of dolomite.

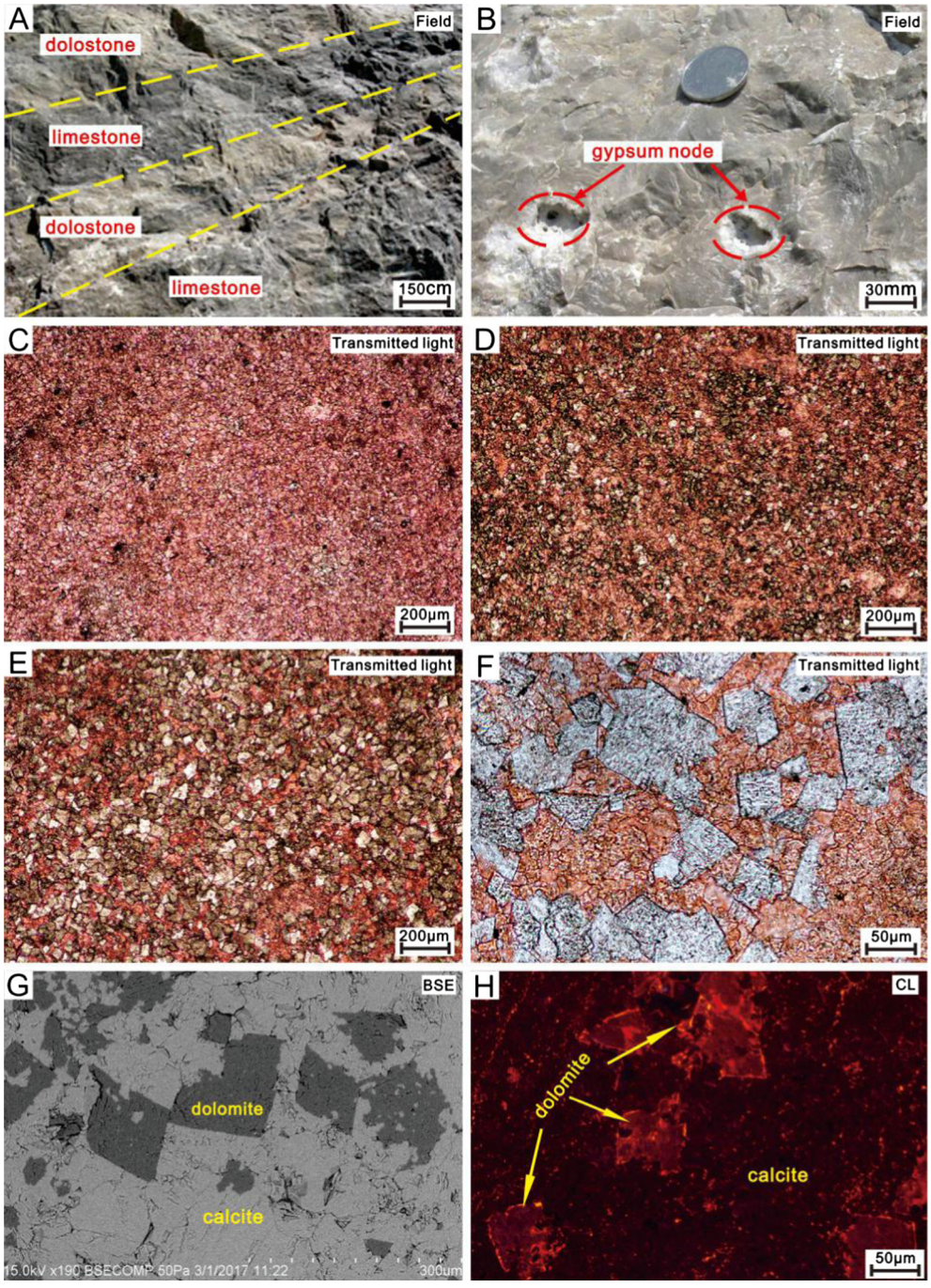

Fig. 3. Photographs showing the petrographic characteristics of Zhoucunchong Formation in Geshan section. (A) Interbedding limestone and dolostone; (B) gypsum node replaced by sparry calcite; (C) limestone (ZC-26); (D) dolomitic limestone (ZC-12), calcite grains show distinct red color due to the stain reaction with Alizarin Red-S and K-Ferricyanide, same as photomicrographs E and F; (E) limy dolostone (ZC-28); (F) dissolution texture of dolomite (ZC-28); (G) back scattered image showing dissolution texture of dolomite (ZC-22) under SEM; (H) cathodoluminescence photomicrograph of dissolution texture of dolomite (ZC-14). (For interpretation of the references to color in this figure legend, the reader is referred to the web version of this article.)

3.2. Geochemical analyses

3.2.1. Element analysis

Each bulk sample was powdered in a pre-cleaned agate mortar and about fifty milligrams of the powder was weighed and subsequently dissolved in 4 mL 7 M HCl in a Teflon beaker as the stock solution. For elemental analyses, a 0.2 mL aliquot of the stock solution was extracted and dried at 99 °C on a hotplate, then treated by adding 0.5 mL concentrated HNO_3 and drying to expel HCl,

before dissolving in 4 mL 2% HNO_3. Concentrations of Ca, Mg, Mn, Fe, Al and Sr for the bulk sample were measured using an inductively coupled plasma optical emission spectrometer (ICP-OES, Thermo Fisher Scientific iCAP 6500 DUO) at School of Earth Sciences and Engineering, Nanjing University. The precision is generally better than ±5% and accuracy is better than ±10% for the selected elements. The remaining stock solution was used for Sr and Mg isotope analyses.

3.2.2. Carbon ($\delta^{13}C$) and oxygen ($\delta^{18}O$) isotope analysis

$\delta^{13}C$ and $\delta^{18}O$ of bulk carbonate powders were measured using a MAT 253 isotope ratio mass spectrometer at Nanjing Institute of Geology and Palaeontology, Chinese Academy of Sciences. All isotope ratios were normalized to the V-PDB standard and reported in per mil (‰). Analytical error (2 standard error or 2SE) is less than 0.03‰ for $\delta^{13}C$ and 0.08‰ for $\delta^{18}O$.

3.2.3. Strontium ($^{87}Sr/^{86}Sr$) isotope analysis

For Sr isotope analyses, 2 mL of the stock solution (dissolved bulk sample powders) was dried down, converted to nitrate form by drying in 0.5 mL concentrated HNO_3, and re-dissolved in 2 mL 3 N HNO_3 for ion exchange purification. Strontium was separated twice using a cation exchange procedure using 100–200 mesh AG50X8 resin (Ling et al., 2007). Strontium isotope ratios were measured using a Finnigan Triton thermo ionization mass spectrometer (TIMS) at the State Key Laboratory for Mineral Deposits Research at Nanjing University. $^{87}Sr/^{86}Sr$ ratios were normalized to $^{86}Sr/^{88}Sr = 0.1194$ using exponential law during each analysis. Repeated measurements of Sr standard NBS987 yielded $^{87}Sr/^{86}Sr = 0.710259 \pm 0.000015$ (2σ, $n = 65$).

3.2.4. Magnesium isotope analysis

Based on the measured Mg content, an aliquot of the stock solution (dissolved bulk sample powders) that contained 50 μg Mg was used for Mg isotope analysis. The sample was treated with 0.5 mL concentrated nitric acid and evaporated on plate at 95 °C, this procedure was repeated three times to convert salts to nitrate form for ion exchange purification. A two-stage ion exchange procedure was used to purify Mg from the samples. The first stage ion exchange procedure is the same as the reported procedure used for K isotope analysis (Li et al., 2016b), that a sample dissolved in 0.5 mL 1.5 N HNO_3 was loaded onto a quartz glass column that contained 1 mL Biorad cation exchange resin AG50W-X12 (100–200 mesh), and eluted using 1.5 N HNO_3 to remove Ca, Na, Al and other cations from Mg. For the second stage column chemistry, the samples were dissolved in 0.5 mL mixed acid (0.2 N HNO_3 + 0.05 N HF) and loaded onto a custom-made Teflon column that contained 0.2 mL Biorad AG50W-X8 (100–200 mesh) cation exchange resin, the resin was successively eluted using the mixed acid (0.2 N HNO_3 + 0.05 N HF), 1 N HNO_3, and 1.5 N HNO_3 to remove K, Ti and remanent Na, Al. After these two column treatments, matrix elements were less than 1% of Mg and recovery was greater than 95%.

Magnesium isotope ratios of the bulk samples were measured using a Thermo Fisher Scientific Neptune Plus MC-ICP-MS at Nanjing University. The instrument was running at low-mass-resolution mode, using a 100 μL/min self-aspirating nebulizer tip and a glass spray chamber. The concentration of samples typically matched the in-house standard to better than ±10%. A 40 s on-peak acid blank was measured before each analysis. Each Mg isotope ratio measurement consisted of fifty 4-s integrations, and the typical internal precision (2 standard error or 2SE) was better than ±0.04‰ for $^{26}Mg/^{24}Mg$ and ±0.02‰ for $^{25}Mg/^{24}Mg$. The long-term external reproducibility (2 standard deviation or 2SD) of Mg isotope analysis is better than ±0.10‰ in $^{26}Mg/^{24}Mg$ and ±0.05‰ in $^{25}Mg/^{24}Mg$ over six months, based on repeat analysis of multiple Mg isotope standard solutions against in-house stock solutions (Appendix Table S1).

All data were normalized to the international Mg isotope standard (DSM3) using conventional δ notation to express per thousand deviations from DSM3:

$$\delta^{26}Mg\ (‰) = (^{26}Mg/^{24}Mg_{sample} - {}^{26}Mg/^{24}Mg_{DSM3}) / (^{26}Mg/^{24}Mg_{DSM3}) \times 1000$$

$$\delta^{25}Mg\ (‰) = (^{25}Mg/^{24}Mg_{sample} - {}^{25}Mg/^{24}Mg_{DSM3}) / (^{25}Mg/^{24}Mg_{DSM3}) \times 1000$$

We used a Mg solution from High Purity Standards Company (Lot No. HPS909104) as the in-house standard for Mg isotope analyses by standard-sample-standard bracketing method. The Mg isotope composition of HPS909104Mg solution relative to international standard DSM3 has been well characterized using two different MC-ICP-MS at University of Wisconsin-Madison for over 5 years ($\delta^{26}Mg = -0.66‰$ relative to DSM3, Li et al., 2011, 2012, 2014, 2015).

The accuracy of Mg isotope measurements is verified by the measured $\delta^{26}Mg$ values for Cambridge 1, a second international Mg isotope standard, which is −2.58 ± 0.11‰ (2SD, $n = 9$), consistent with published values (e.g., −2.58 ± 0.14‰, Galy et al., 2003; −2.58 ± 0.04‰, Hippler et al., 2009; −2.57 ± 0.12‰, Li et al., 2012; −2.62 ± 0.03‰, Teng et al., 2015).

To verify the accuracy of chemical procedure, IAPSO seawater standard and three USGS rock standards (BHVO, DST-2, BIR) were processed along with samples in the ion-exchange procedure. The measured $\delta^{26}Mg$ values of the standard samples match the published values within ±0.10‰, and mostly within ±0.05‰ (Appendix Table S1).

4. RESULTS

4.1. Petrography and mineralogy

Limestone outcrops at the Geshan show dark gray color, whereas dolostone show light gray color and they interbed each other (Fig. 3A). Gypsum concretions and nodes occur in dolostone layers (Fig. 3B). Detailed microscope and SEM observations on the thin sections of the carbonate rocks confirmed the lack of any microscopic features of secondary weathering (porosity, secondary min-

erals) in the carbonate rocks. Irrespective of calcite to dolomite ratios, the carbonate samples consistently show microcrystalline textures (Fig. 3C–E), composed of 20–30 μm sized calcite crystals and 25–50 μm sized dolomite crystals. The dolomite crystals are mostly subhedral in shape (Fig. 3E–H), but the etched edges of some dolomite crystals (Fig. 3F–H) indicate dissolution of the originally more euhedral dolomite crystals, implying that a process of dedolomitization may have taken place after the formation of dolomite crystals.

Powder XRD analyses of bulk sample powders show that the dolomite components are almost stoichiometric, containing 48.2–50.0 mol% $MgCO_3$, and have a limited dispersion in degree of order $[R = I(015)/I(110)]$ that ranges between 0.34 and 0.51 (Appendix Table S2). The calcite components of the carbonate samples have tightly distributed d_{104} values (3.028–3.031, mostly 3.029), which correspond to 1.17 mol% of $MgCO_3$ in calcite (Appendix Table S2). The homogeneity of mineral chemistry in both calcite and dolomite is in sharp contrast to the large variation in relative proportion of the two minerals among the carbonate samples from the Geshan section.

4.2. Major and trace elements

Magnesium contents of the bulk rock samples vary remarkably, from 0.28 to 10.60 wt%, and the variations in Mg contents are mirrored by changes in Ca contents that varies from 24.54 to 39.07 wt% (Appendix Table S3, Fig. 2), reflecting that the relative abundance of calcite and dolomite is the main control of bulk rock chemistry. The relative proportions of dolomite and calcite are calculated using both the measured Mg and Ca concentrations and the (104) peaks of dolomite and calcite measured by XRD, and data from the two methods match well (Appendix Table S4, Fig. 2). Strontium concentrations in carbonates decrease rapidly with increasing Mg concentrations, from 3471 ppm in limestone to 150 ppm in dolostone (Fig. 4a). By contrast, Mn concentrations increase with increasing Mg contents (Fig. 4b). Magnesium contents do not show correlation with Fe or Al contents (Appendix Table S3), but there is a significant positive correlation between Fe and Al contents (Fig. 4c). In a cross-plot of Fe-Al contents, the majority of data plot along a trend that corresponds to upper continental crust values (Fe/Al = 0.48: Rudnick and Gao, 2003), with exceptions of only a few high Fe samples, reflecting that these two elements are mostly detrital in origin.

4.3. Isotope geochemistry

Carbonates from Geshan section have bulk-rock $\delta^{13}C$ (V-PDB) values ranging from 4.2‰ to 6.6‰ (Appendix Table S5, Fig. 2) and these are consistent with the $\delta^{13}C$ values of early Anisian seawater which ranges from 4.0‰ to 5.5‰ as summarized from previous stratigraphy studies (Korte et al., 2005; Ovtcharova et al., 2015). $\delta^{18}O$ (V-PDB) values range from −6.4‰ to −10.4‰ (Appendix Table S5, Fig. 2). Despite remarkable scatter in the dataset, calcite-rich samples tend to have slightly higher $\delta^{13}C$ and $\delta^{18}O$ values than the dolomite-rich samples. And there is a positive correlation between $\delta^{13}C$ and $\delta^{18}O$ values (Fig. 5).

$^{87}Sr/^{86}Sr$ ratios of the bulk samples range from 0.70801 to 0.70837 and show a significant positive correlation with Mg contents (Fig. 6a) and a negative correlation with Sr contents (Fig. 6b). For comparison, $^{87}Sr/^{86}Sr$ ratios of early Anisian seawater are suggested to be 0.70780–0.70820 (Korte et al., 2003).

$\delta^{26}Mg$ values of the samples vary significantly, from −2.28‰ in limestone to −1.43‰ in dolomite-rich carbonates (Appendix Table S5, Fig. 7a).

5. DISCUSSION

5.1. End member mixing in the Geshan section carbonates

Despite large variations in major and trace element compositions in bulk samples, XRD analyses demonstrate the chemical homogeneity of dolomite and calcite in all Geshan samples (Appendix Table S4). This, together with

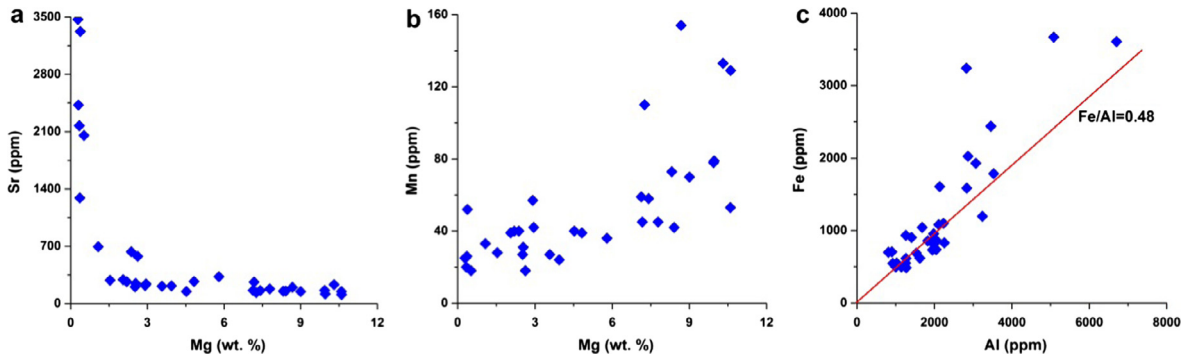

Fig. 4. Cross plots of elemental data of the Geshan carbonates. (a) Cross-plot of Sr contents versus Mg contents; (b) cross-plot of Mn contents versus Mg contents; (c) cross-plot of Fe and Al contents, and the red line is the reference line making the Fe/Al ratio of continental crust (Rudnick and Gao, 2003). (For interpretation of the references to color in this figure legend, the reader is referred to the web version of this article.)

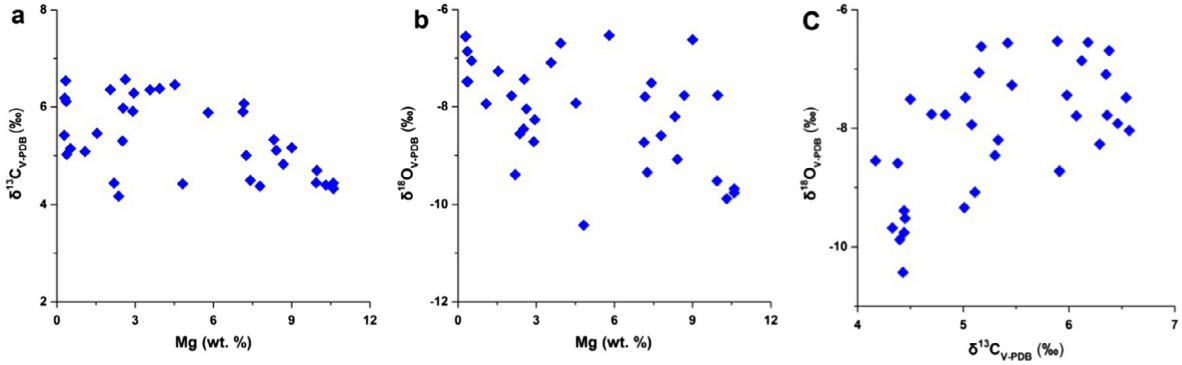

Fig. 5. (a) Cross-plot of $\delta^{13}C_{V\text{-}PDB}$ values versus Mg contents of bulk samples; (b) cross-plot of $\delta^{18}O_{V\text{-}PDB}$ values versus Mg contents of bulk samples; (c) cross-plot of $\delta^{13}C_{V\text{-}PDB}$ values versus $\delta^{18}O_{V\text{-}PDB}$ values.

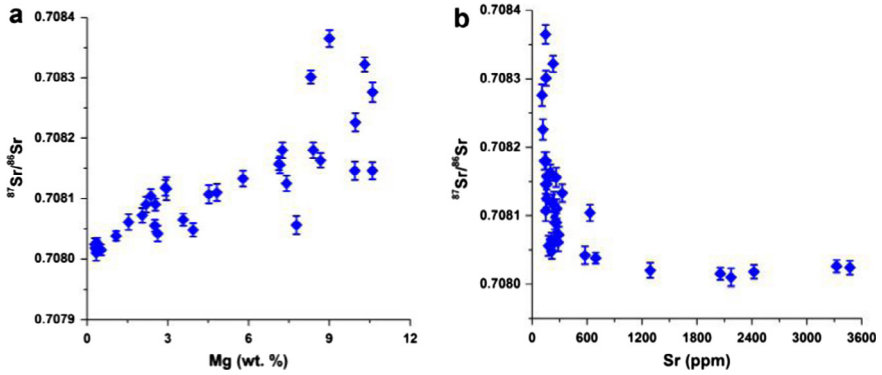

Fig. 6. Cross plots of isotopic ratios versus elemental contents. (a) Cross-plot of $^{87}Sr/^{86}Sr$ ratios versus contents of bulk samples; (b) cross-plot of $^{87}Sr/^{86}Sr$ ratios versus Sr contents.

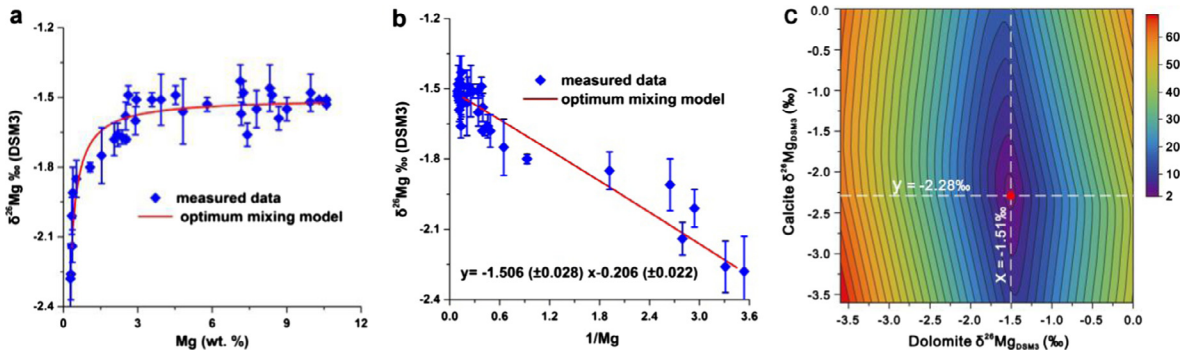

Fig. 7. (a) Plot of $\delta^{26}Mg$ values versus Mg contents. The solid lines show the mixing trend of end members defined from the best fitting line; (b) plot of $\delta^{26}Mg$ values versus 1/Mg values. Red solid line denotes the least squares fitting of the measured data; (c) color contour plot of the optimization model, which shows the fitting of two end member mixing with the measured data. The end member $\delta^{26}Mg$ values calculated from the optimization model is consistent with those obtained from the least squares fitting in Fig. 7b, within statistical uncertainty. (For interpretation of the references to color in this figure legend, the reader is referred to the web version of this article.)

the textural homogeneity in individual carbonate layers (Fig. 2) as observed from microscopy, provides the basis for the two end-member mixing concept. Cross-plots of Sr versus Mg contents also support two end member mixing (Fig. 4a), this, together with the positive correlation between Mn and Mg as shown in Fig. 4b, indicate calcite has low Mn content and high Sr content whereas dolomite has high Mn content and low Sr content. The higher $^{87}Sr/^{86}Sr$ ratios of dolomite-rich carbonates (Fig. 6a), however, are attributed to relatively higher contributions of radiogenic ^{87}Sr in the low Sr dolostone samples, whereas carbonates with high Sr concentrations are considered to be less impacted by radioactive decay of ^{87}Rb from detrital components (Elderfield, 1986; McCormack et al., 2015).

Magnesium isotope compositions in Geshan carbonates also show distinct feature of two end member mixing, as indicated by the linear relation between Mg isotope ratios and the reciprocal of Mg contents (Fig. 7b). XRD analyses (see "methods" for details) show that the calcite end member has a stoichiometry of $Ca_{0.9883}Mg_{0.0117}CO_3$ and the dolomite end member has an ideal stoichiometry ($CaMg(CO_3)_2$) (Appendix Table S2), and the samples are composed of the only two Mg-bearing minerals. The Mg isotope compositions for the two end members could be obtained by intercepting vertical lines representing dolomite and calcite end members with the least-squares best fitting line in Fig. 7b. Using this method, $\delta^{26}Mg$ of calcite and dolomite end members are calculated at $-1.52 \pm 0.04‰$ and $-2.24 \pm 0.12‰$ respectively (Fig. 7a and b).

In addition, we used an independent optimization approach to derive the end member $\delta^{26}Mg$ values. In this approach, we set hypothetical $\delta^{26}Mg$ values for calcite and dolomite end members, which can be used to calculate the modeled $\delta^{26}Mg$ value for each bulk sample, based on proportion of calcite and dolomite in each sample calculated from XRD or bulk chemistry data (Appendix Table S4), and for each sample we calculated the residue (absolute difference, or $abs[\delta^{26}Mg_{i\text{-modeled}} - \delta^{26}Mg_{i\text{-measured}}]$) between modeled and measured $\delta^{26}Mg$ values. We can calculate the sum of residue for all samples ($R = \sum abs[\delta^{26}Mg_{i\text{-modeled}} - \delta^{26}Mg_{i\text{-measured}}]$), given a pair of pre-defined $\delta^{26}Mg$ values for calcite and dolomite end members. Such optimization approach allows searching of the optimum in a two dimensional space of possible $\delta^{26}Mg$ values for calcite and dolomite end members. The optimum $\delta^{26}Mg$ values for dolomite end member and calcite end member correspond to the lowest sum of residue are $-1.51‰$ and $-2.28‰$ respectively (Fig. 7c).

Both methods show a similar difference of $\delta^{26}Mg$ values between the calcite end member and the dolomite end member. Because Gauss–Markov theory suggests higher robustness for the least-squares method, we use the $\Delta^{26}Mg_{dolo\text{-}calc} = 0.72 \pm 0.13‰$ as obtained from the least-squares method in the following discussion. Note that this value is substantially lower than the Mg isotopic difference between dolomite and calcite measured in Peng et al. (2016), where $\Delta^{26}Mg_{dolo\text{-}calc} = 1.6‰$. The origin of such difference is discussed in the following section.

5.2. Post-depositional processes and the isotopic response of Mg

Multiple lines of evidence consistently shows that carbonates from Geshan section had been affected by post-depositional processes. Regionally, the strata underwent burial processes and previous studies on strata burial and thermal history of the adjacent Jurong Block in the studied region indicated that Triassic strata reached a maximum depth beyond 3500 m in the Late Cretaceous and experienced a peak burial temperature of about 140 °C (Appendix Fig. S2; Hua, 2014; Huang et al., 2014). This is consistent with the hydrocarbon charging event in the region and the homogenization temperature of the corresponding hydrocarbon inclusions is about 145 °C (Liu et al., 2005). $\delta^{18}O_{V\text{-}PDB}$ values of the carbonates are relatively depleted (Fig. 5b and c), indicating oxygen isotope compositions of carbonates were overwritten by fluids in burial stage after dolomitization (Hodgson, 1966). On the other hand, the consistency between Sr isotope signatures of carbonates and Anisian seawater is consistent with the absence of activity of fluids of magmatic origin throughout the post-depositional history of the Geshan section, supporting that the thermal event was purely burial in nature. Petrographically, dolomite grains commonly show textures of dissolution and erosion (Fig. 3F–H), also indicating a fluid event after dolomite formation. Considering the large volume of gypsum in the upper Zhoucunchong Formation (Fig. 1B), significant volume of water could be released during the subsiding stage with increasing burial temperature, based on the calcium sulfate dehydration reaction sequence $CaSO_4{\cdot}2H_2O \rightarrow \beta\text{-}CaSO_4{\cdot}0.5H_2O \rightarrow \gamma\text{-}CaSO_4$ (Molony and Ridge, 1968; Vakhlu et al., 1985). Notably, $CaSO_4{\cdot}2H_2O$ completely transforms to $\gamma\text{-}CaSO_4$ at temperatures above 115 °C (Ball and Norwood, 1969). Gypsum dehydration could have provided fluids that aided isotopic resetting of carbonates.

The evidence above suggests that the carbonate minerals from the Geshan section have been reset during post-depositional processes during burial, which could have also modified the isotopic signatures of Mg in the system. Indeed, theory of stable isotope fractionation predicts that the magnitude of isotope fractionation decreases as the temperature increases (Urey, 1947). The 0.72‰ difference in $\delta^{26}Mg$ between the dolomite end member and the calcite end member of Geshan section is remarkably smaller than the 1.6‰ difference in $\delta^{26}Mg$ between calcite and dolomite in the study of Peng et al. (2016) that was interpreted to reflect precipitation at a low temperature (Fig. 8). Therefore a 0.72‰ difference in $\delta^{26}Mg$ between the dolomite end member and the calcite end member most likely reflects inter-mineral Mg isotope fractionation at an elevated temperature during post-depositional processes, and the primary difference in $\delta^{26}Mg$ between the two minerals should be significantly greater and might be close to a value of 1.6‰ as reported in Peng et al. (2016).

Magnesium isotope fractionation factors for carbonate minerals have been investigated by a number of workers, using approaches of theoretical calculation (Rustad et al., 2010; Schauble, 2011; Pinilla et al., 2015), or experimental calibration (Li et al., 2012, 2015; Pearce et al., 2012; Mavromatis et al., 2013; Wang et al., 2013). Large discrepancies, however, exist between the available studies. These are illustrated by the inter-mineral Mg isotope fractionations between calcite and dolomite ($\Delta^{26}Mg_{dolo\text{-}calc}$, Fig. 8). Large temperature effect was predicted for $\Delta^{26}Mg_{dolo\text{-}calc}$ (Rustad et al., 2010; Pinilla et al., 2015) in theoretical calculations. $\Delta^{26}Mg_{dolo\text{-}calc}$ can also be derived from experimentally calibrated Mg isotope fractionation factors between carbonate minerals and aqueous solutions, and by combining the experimental studies for dolomite (Li et al., 2015) and calcite (Mavromatis et al., 2013; Saenger and Wang, 2014). The experimental study of Mavromatis et al. (2013) is preferred over other studies (Li et al., 2012; Saulnier et al., 2012) on calcite due to the better control

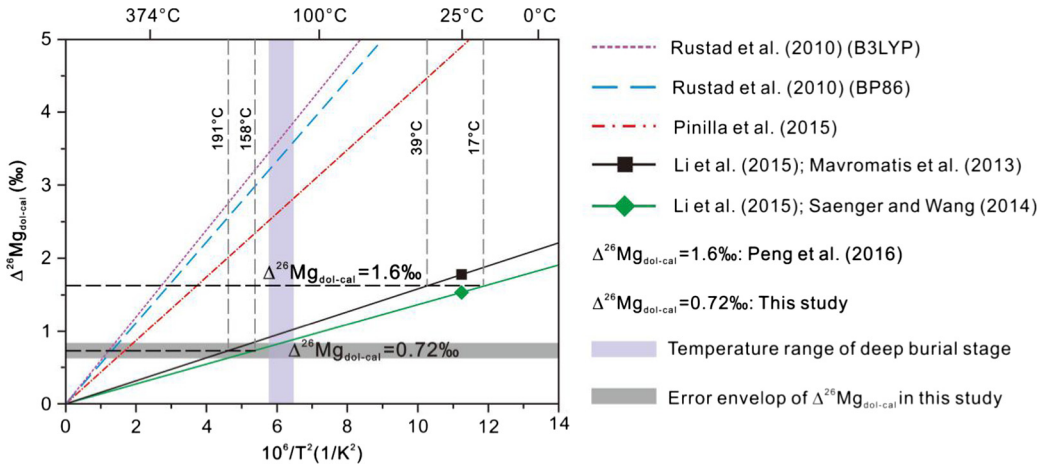

Fig. 8. Compilation of Mg isotope fractionation factors between dolomite and calcite as a function of $1/T^2$ in different studies. Red, Purple and blue lines denote fractionation factors calculated by Pinilla et al. (2015) and Rustad et al. (2010) using different models. In addition, experimental results for dolomite (Li et al., 2015) and calcite (Mavromatis et al., 2013 and Saenger and Wang, 2014) are combined and extrapolated to higher temperatures using a $1/T^2$ function. Shadowed squares mark the ranges of burial temperature and inter-mineral Mg isotope fractionation at the Geshan section. The peak burial temperature of Geshan carbonate is about 140 °C as estimated based on the strata burial history by Hua (2014) and Huang et al. (2014). (For interpretation of the references to color in this figure legend, the reader is referred to the web version of this article.)

of kinetic isotope effects in the study of Mavromatis et al. (2013). Experimentally determined Mg isotope fractionation factors are extrapolated to higher temperatures using a $1/T^2$ relation (Fig. 8), which is a common practice in stable isotope geochemistry (Li et al., 2011; Young et al., 2015).

The well-constrained thermal history and Mg isotope fractionation factors between dolomite and calcite end members provide a valuable opportunity to resolve the current controversy on Mg isotope fractionation factors between calcite and dolomite. Because rate of isotopic exchange increases exponentially with increasing temperature (Cole and Chakraborty, 2001), the $\Delta^{26}Mg_{dolo\text{-}calc}$ we measured from Geshan section most likely reflects Mg isotope equilibrium at the maximum burial temperature of 145 °C. Particularly, phase transformation from γ-$CaSO_4$ back to $CaSO_4{\cdot}2H_2O$ would consume any free H_2O and suppress fluid activity during the retrograde metamorphism, therefore Geshan section would remained dry during uplifting after burial peak, and isotopic exchange without fluid is much more sluggish than with the presence of fluid. As shown in Fig. 8, the $\Delta^{26}Mg_{dolo\text{-}calc}$ fractionation and temperature data for Geshan section plot well below the lines of theoretical calculations, but is more consistent with the experimentally calibrated T-$\Delta^{26}Mg_{dolo\text{-}calc}$ trend. It is also important to note that the data ($\Delta^{26}Mg_{dolo\text{-}calc}$ = 1.6‰) of Peng et al. (2016) also plot along the experimentally calibrated T-$\Delta^{26}Mg_{dolo\text{-}calc}$ trend, but at a lower temperature. Peng et al. (2016) suggested that both calcite and dolomite in their study formed near the seawater–sediment interface (about 25 °C). This would imply that the carbonate minerals from samples in Peng et al. (2016) remained un-altered throughout the geological history. Isotopic difference of Mg between calcite and dolomite pairs, therefore, may be useful to distinguish the thermal history of carbonates, and help to identify alteration events in carbonates. In some cases (this study for example), Mg isotopic difference between calcite and dolomite pairs could be used as geothermometer, although the sensitivity of $\Delta^{26}Mg_{dolo\text{-}calc}$ as geothermometer decreases rapidly at temperatures above 150 °C (Fig. 8).

5.3. Applicability of Mg isotopes in carbonate minerals as seawater proxy

The potential of Mg isotope composition in carbonates as a tracer of seawater chemistry through geological history has attracted great interests (Hippler et al., 2009; Pogge von Strandmann et al., 2014; Li et al., 2015; Geske et al., 2015b; Riechelmann et al., 2016; Rollion-Bard et al., 2016). To use $\delta^{26}Mg$ of carbonates as a proxy to study coeval sea water, two important pre-requisites of carbonate minerals need to be satisfied: (1) magnesium isotopes in carbonate minerals were in equilibrium with the coeval seawater, and (2) magnesium isotopic signatures in carbonate minerals remained conservative against post-depositional alterations. Comprehensive geochemical data from the Geshan section allows a detailed assessment of these two aspects of Mg isotopes in carbonates as seawater proxy.

5.3.1. Robustness of Mg isotope record in calcite and dolomite

Post-depositional processes are ubiquitous for sedimentary rocks, and as discussed in the previous section, resetting of Mg isotopes between dolomite and calcite could occur during burial processes at a temperature as low as 150 °C. Using the calculated proportions of calcite in bulk rock samples from each carbonate layer (Appendix Table S4), and the measured thickness of the 26 individual layers (Fig. 2), we calculated that the Geshan section

comprises 26 mol% dolomite and 74 mol% calcite. Combining the stoichiometry of dolomite and calcite measured by XRD, we further calculated that 97% of Mg in the Geshan section exists in dolomite, and only 3% of Mg in the section occurs in calcite. The relative sensitivity of Mg isotopes in calcite and dolomite against resetting is evaluated as below in two extreme scenarios, one is completely closed, and the other is completely open, and natural processes may be somewhere between the two extreme scenarios. In a completely closed system scenario, because the overwhelming majority of Mg exists in dolomite, when re-equilibration of Mg isotopes occurred between calcite and dolomite during burial metamorphism, the Mg isotope mass balance would be controlled by dolomite rather than calcite. Therefore, δ^{26}Mg of dolomite changed little, whereas δ^{26}Mg of calcite shifted toward δ^{26}Mg of dolomite in response to increasing temperature in the fluid-rock interactions, through in-situ dissolution-precipitation (recrystallization) processes even without significant input of external fluids. In an open system scenario such as resetting by fluids released from compaction and dewatering of clay-rich successions below the carbonate formation, the higher Mg content in dolomite than calcite means that given the same intensity of secondary fluid alteration (e.g., Mg addition or Mg exchange), dolomite would be less susceptible to Mg isotope change than calcite. Therefore, from a mass balance point of view, dolomite is more robust in retaining the original Mg isotope signature, irrespective of open system or closed system behavior of the carbonates. This is in agreement with Azmy et al. (2013) and Geske et al. (2012) who suggested that Mg isotopes in dolomite tend to be conservative.

Additionally, previous studies have shown that high Mg calcite and aragonite of marine origin are thermodynamically unstable (Friedman, 1965; Aissaoui, 1988; Bischoff et al., 1993) and have a tendency to recrystallize and transform to low-Mg calcite even at a low temperatures (Aissaoui, 1988; Bertram et al., 1991; Bischoff et al., 1993). Hydrothermal alteration experiments of brachiopod shell indicated that even for low-Mg calcite that has relatively higher thermodynamic stability, δ^{26}Mg values are still sensitive to diagenetic alterations (Riechelmann et al., 2016). Stoichiometric dolomite as confirmed from the Geshan section, by contrast, is a thermodynamically stable mineral under a wide range of physical-chemical conditions (Rosenberg and Holland, 1964; Alruopn, 1977; Katz and Matthews, 1977; Carpenter, 1980). Thermodynamics therefore favors stoichiometric dolomite as the more robust mineral recorder. It should be noted that Gao et al. (2016) reported dissolution of dolomite and precipitation of calcite and accompanied Mg isotope fractionation in a surface dolostone sample. The case as reported by Gao et al. (2016), however, comes from a long-exposed rock surface with presence of silicates that has been intensely weathered by copious meteoric water, and it is not clear whether this is a universal phenomenon that applies to unweathered dolostones. By contrast, in a more relevant case, Jacobson et al. (2010) reported that δ^{26}Mg values of ground water in the dolomite-dominant Madison Aquifer of United States remain invariant along the flow path for ~170 km. The best and most straightforward explanation is the lack of Mg isotope fractionation during dolomite weathering, attesting to the robustness of dolomite as a Mg isotope reservoir.

Finally, given that intergrowth texture is common in carbonates, from an analytical point of view, Mg isotope composition of pure calcite mineral is usually difficult to measure from natural carbonate rocks because Mg in calcite is prone to influence of impurities of Mg rich minerals such as dolomite. This is clearly demonstrated in Fig. 7a, that δ^{26}Mg of calcite-rich bulk rock samples increases dramatically with a small increase in Mg content. By contrast, δ^{26}Mg of dolomite rich samples is insensitive to existence of calcite in the bulk samples (Fig. 7a).

In short, we argue that dolomite is a more robust mineral than calcite as an archive of Mg isotopes. Caution is therefore needed when using Mg isotopes in calcite to reconstruct ancient seawater chemistry. Pogge von Strandmann et al. (2014) analyzed Mg-calcite in pelagic foraminifers and proposed a seawater δ^{26}Mg curve for the past 40 Myr. In a similar approach, Higgins and Schrag (2015) measured Mg isotope compositions of bulk pelagic carbonates over the last 75 Myr. However, there is considerable inconsistency in reconstructed seawater δ^{26}Mg curves between the two studies (Fig. 9). Considering the homogeneity of Mg isotopes in open ocean seawater (Ling et al., 2011), the difference in reconstructed δ^{26}Mg of seawater in the last 40 Myr between the studies of Pogge von Strandmann et al. (2014) and Higgins and Schrag (2015) seems to be best explained by either post-depositional alterations to at least some of the measured low Mg-calcite samples, or the lack of equilibrium Mg isotope fractionation during precipitation of low Mg-calcite in at least some of the samples.

5.3.2. Dolomite: an effective archive of δ^{26}Mg of coeval seawater?

Given the greater robustness of Mg isotopes in dolomite than calcite against post-depositional processes, questions about the applicability of Mg isotopes in carbonate sedimentology center on whether we can derive Mg isotope signature of ancient seawater from dolomite. First we consider the source of Mg for dolomite. The possible Mg sources for dolomite include (1) hydrothermal fluids (Davies and Smith, 2006; Gasparrini et al., 2006; Lapponi et al., 2014), (2) clay mineral transformation (McHargue and Price, 1982) and compaction waters coming from shale (Machel and Anderson, 1989; Kırmacı and Akdağ, 2005), and (3) coeval sea water or evolved/modified seawater (Dickson et al., 2001; Qing et al., 2001). In case of the Geshan section, the lack of occurrence of large-scale igneous rocks and skarn in the sampling area rules out the possibility of hydrothermal Mg supply. On the other hand, 943 cm^3 of shale would be needed to dolomitize 1 cm^3 of calcite, according to Machel and Anderson (1989). Although shales occur in the Lower Triassic strata below the Zhoucunchong Formation at Geshan (Fig. 1B), the volume is not significant enough relative to the mass of dolomite in Zhoucunchong Formation. In addition, calcite layers within the Lower Triassic shale strata are not dolomitized (Fig. 1B). Therefore Mg in Zhoucunchong

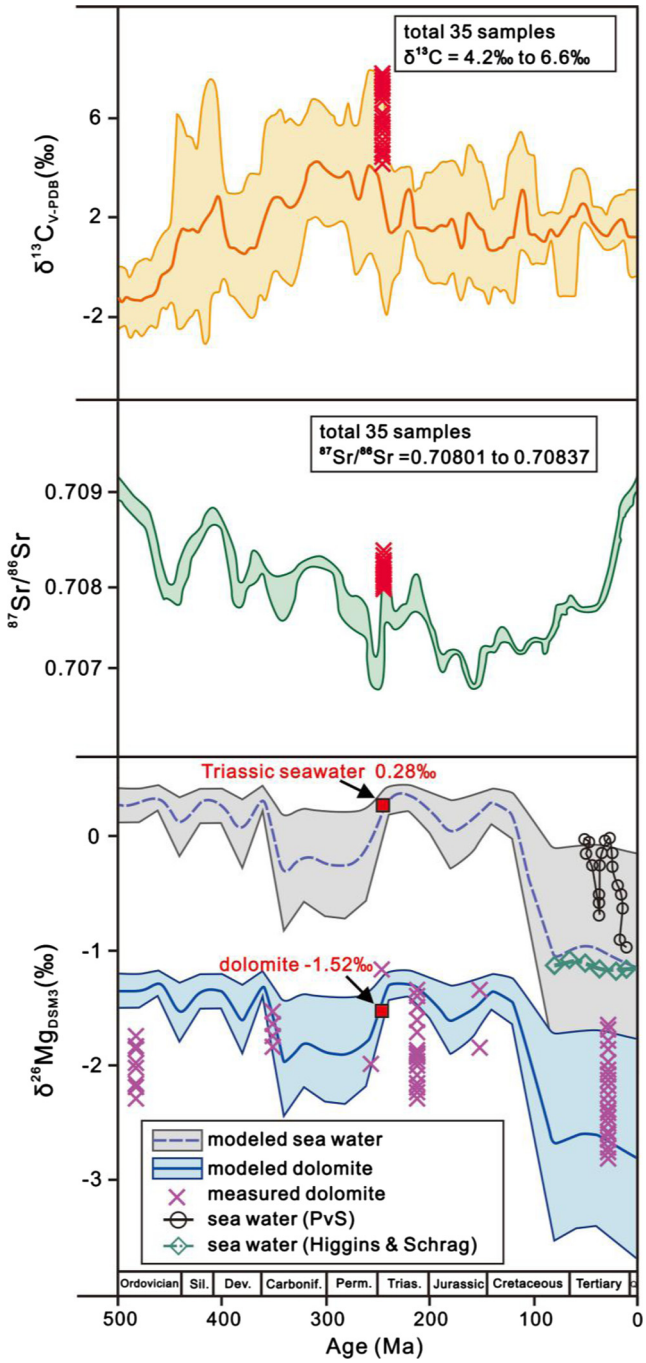

Fig. 9. Comparisons of measured $\delta^{13}C$, $^{87}Sr/^{86}Sr$, data from Geshan section, and the proposed $\delta^{13}C$, $^{87}Sr/^{86}Sr$ values of seawater over the Phanerozoic, as well as a comparison of $\delta^{26}Mg$ of dolomite end member from the Geshan section and corresponding seawater, with the proposed $\delta^{26}Mg$ values for massive dolomite and seawater over the Phanerozoic. Seawater $\delta^{13}C$, $^{87}Sr/^{86}Sr$ data are from Veizer et al. (1999), and the $\delta^{26}Mg$ values of massive dolomite and seawater are from Li et al. (2015). Mg isotope compositions of Phanerozoic massive dolomite are reported by Azmy et al. (2013), Blättler et al. (2015), Fantle and Higgins (2014), Geske et al. (2012), Jacobson et al. (2010), and Mavromatis et al. (2014). The seawater $\delta^{26}Mg$ curve over the past 40 Ma as proposed by Pogge von Strandmann et al. (2014) is plotted for comparison. In addition, Higgins and Schrag (2015) measured $\delta^{26}Mg$ values of pelagic carbonate over the past 75 Ma, and a seawater $\delta^{26}Mg$ curve is derived from the results of Higgins and Schrag (2015) by assuming $\Delta^{26}Mg_{calcite\text{-}solution}$ of −3.5‰ at 25 °C (Mavromatis et al., 2013).

Formation cannot be provided from shale and clay diagenesis. This is consistent with the modeling results of Li et al. (2016a), who suggested that clay minerals in marlstones are not able to provide enough Mg^{2+} for massive dolomitization. Finally, seawater is the only reservoir that can provide sufficient Mg in massive dolomite (Sun, 1994; Qing et al., 2001; Kırmacı, 2008; Rameil, 2008). Previous studies on local sedimentology and paleogeography indicated

development of carbonate platforms in the lower Yangtze Region of eastern China during the Middle Triassic (Tong and Yin, 1997), which facilitated production of penesaline–hypsaline seawater by evaporation and formation of syngenetic–penecontemporaneous dolomites (Qing et al., 2001; Rameil, 2008). Seawater evaporation is confirmed by occurrence of gypsum in the strata (Fig. 2B). We conclude that Mg in carbonates in Geshan section ultimately originated from modified (evaporated) seawater. Our conclusion is further supported by the agreement in $^{87}Sr/^{86}Sr$ and $\delta^{13}C$ between the Geshan carbonate samples and the coeval seawater (Veizer et al., 1999; Korte et al., 2003), as demonstrated in Fig. 9.

Based on the seawater origin of Mg in dolomite from the Geshan section, we further discuss whether Mg isotope fractionation occurred during dolomite precipitation. It has been reported by Geske et al. (2015b) that $\delta^{26}Mg$ of modern sabkha dolomite has $\delta^{26}Mg$ value of $-0.79 \pm 0.41‰$, close to that of seawater ($-0.8‰$: Ling et al., 2011), reflecting inadequate Mg exchange between dolomite and seawater and the lack of equilibrium Mg isotope fractionation during sabkha dolomite precipitation. In contrast, a ca. 2‰ fractionation between dolomite and aqueous solution is inferred from experiments and ODP drill cores (Fantle and Higgins, 2014; Li et al., 2015). A dolomitization process without Mg isotope fractionation does not apply to the Geshan section, because the $\delta^{26}Mg$ value of dolomite is low ($-1.52‰$). Such value is lower than that of global riverine input into oceans ($-1.09‰$: Tipper et al., 2006). Average $\delta^{26}Mg$ of global riverine input is unlikely to have changed dramatically in the Phanerozoic, and $\delta^{26}Mg$ of seawater should be higher than that of riverine input due to the important sink of isotopically light Mg into carbonates (Tipper et al., 2006). Therefore $\delta^{26}Mg$ values of the Phanerozoic seawater should be higher than $-1.09‰$ unless a large Mg sink with opposite Mg isotope fractionation exists, and in light of this, Mg isotope fractionation should have occurred between dolomite and coeval seawater during formation of Geshan carbonates.

As discussed above, Mg in Geshan section carbonates originated from coeval seawater and Mg isotope fractionation occurred during formation of carbonates, but can we use the $\delta^{26}Mg$ values of dolomite to reconstruct Mg isotope compositions of ancient seawater? Dolomitization process is complicated and the behavior of Mg isotopes during dolomitization at low temperature is still not fully understood. Although equilibrium Mg isotope fractionation factors have been proposed based on experiments and field observations (Fantle and Higgins, 2014; Li et al., 2015), non-equilibrium processes like kinetic isotope effects during dolomitization remain under-explored. It is not known whether kinetic isotope signatures in primary dolomite precipitates can be erased by later recrystallization during early burial processes over geological timescales. An additional source of complexity is that Mg isotope composition of pore fluids may also evolve in respond to dolomitization, which produces dolomite that is not in equilibrium with seawater. The isotopic effects of such process have been studied theoretically by Huang et al. (2015) based on a Diffusion-Advection-Reaction model, which indicated that Mg isotope composition of bulk carbonate rocks should change systematically across a dolomitization front (or diffusion profile). The highly variable and irregular calcite/-dolomite ratios across the Geshan section (Fig. 2), however, show that a vertical dolomitization/diffusion front cannot be identified across the strata, therefore the Diffusion-Advection-Reaction model by Huang et al. (2015) does not seem to be applicable to the case of this study. Finally, despite all the complexities in regard to Mg isotope fractionation during dolomitization as discussed above, Li et al. (2015) calculated curves of $\delta^{26}Mg$ values for seawater and massive dolomite throughout the Phanerozoic based on an isotope mass balance model and data of intensity of dolomitization in geological history (Wilkinson and Algeo, 1989). In the model of Li et al. (2015), an equilibrium $\Delta^{26}Mg_{dolo\text{-}aq}$ fractionation of $-1.8‰$ is assumed between massive dolomite and seawater. As shown in Fig. 9, the measured $\delta^{26}Mg$ for dolomite from Geshan agrees with the modeled $\delta^{26}Mg$ value for dolomite well. Such agreement implies that dolomite in Geshan section might be in equilibrium with coeval seawater, and therefore, dolomite in Geshan section is likely to be syndepositional in origin, which allowed adequate Mg isotope exchange between carbonate precipitates and coeval seawater. Therefore, irrespective of its origin (e.g., direct precipitates from seawater or replacement of seawater in early diagenesis), syndepositional massive dolomite may reasonably record Mg isotope composition of coeval seawater. Nonetheless, we stress that further work is needed to check whether the modeled $\delta^{26}Mg$ values of dolomite by Li et al. (2015) match those of geological records and to rigorously test whether massive syndepositional dolomite can be used as an effective archive of Mg isotope compositions of ancient seawater.

6. CONCLUSION

The Middle Triassic Geshan section in the Lower Yangtze Block consists of carbonate of variable dolomite to calcite ratios and has a well-constrained burial history, which is ideal for investigation of Mg isotope behaviors during post-depositional processes. The carbonates contains only dolomite and calcite, and the two minerals demonstrate chemical and textural homogeneity. Magnesium isotope compositions of the bulk carbonate rocks closely follow a mixing trend between a high $\delta^{26}Mg$ dolomite end member and a low $\delta^{26}Mg$ calcite end member. An inter-mineral $\Delta^{26}Mg_{dolomite\text{-}calcite}$ fractionation of 0.72‰ was obtained after deconvolving the end member Mg isotope compositions. Using the experimentally derived Mg isotope fractionation factors for dolomite and calcite, a temperature of 150–190 °C was calculated to correspond the 0.72‰ $\Delta^{26}Mg_{dolomite\text{-}calcite}$ fractionation, and such temperature range matches well with the burial-thermal history of the local strata, making a successful case of Mg isotope geothermometry and revealing Mg isotope re-equilibration at a relative higher temperature after dolomitization. Mass balance calculation shows that because the overwhelming majority of Mg existed in dolomite, the system was buffered by dolomite rather than calcite during

resetting of Mg isotopes in burial stages. Furthermore, considering the higher thermodynamic stability of dolomite than Mg-bearing calcites, Mg isotopes in dolomite are more robust against post-depositional alterations. Measured Mg isotope compositions for dolomite end member of Geshan section matches with the modeled Mg isotope curve for Phanerozoic massive dolomite as proposed by Li et al. (2015), supporting the idea that massive syndepositional dolomite could be used to reconstruct the Mg isotope compositions of ancient seawater.

ACKNOWLEDGMENTS

This manuscript benefits from constructive reviews from Adrian Immenhauser, Josh Wimpenny and an anonymous reviewer. We also thank Prof. Andrew Jacobson for his editorial handling and constructive comments. This study is supported by the National Science Foundation of China (Nos. 41473002 and 41561144002 to W.L.; No. 41230312 to H.W.).

APPENDIX A. SUPPLEMENTARY MATERIAL

Supplementary data associated with this article can be found, in the online version, at http://dx.doi.org/10.1016/j.gca.2017.03.026.

REFERENCES

Aissaoui D. M. (1988) Magnesian calcite cements and their diagenesis: dissolution and dolomitization, Mururoa Atoll. *Sedimentology* **35**, 821–841.

Allan J. R. and Matthews R. K. (1982) Isotope signatures associated with early meteoric diagenesis. *Sedimentology* **29**, 797–817.

Alruopn P. L. (1977) Structural refinements of dolomite and a magnesian calcite and implications for dolomite formation in the marine environment. *Am. Miner.* **62**, 772–783.

Azmy K., Lavoie D., Wang Z., Brand U., Al-Aasm I., Jackson S. and Girard I. (2013) Magnesium-isotope and REE compositions of Lower Ordovician carbonates from eastern Laurentia: implications for the origin of dolomites and limestones. *Chem. Geol.* **356**, 64–75.

Ball M. C. and Norwood L. S. (1969) Studies in the system calcium sulphate–water. Part I. Kinetics of dehydration of calcium sulphate dihydrate. *J. Chem. Soc. A.*, 1633–1637.

Banner J. L. (1995) Application of the trace element and isotope geochemistry of strontium to studies of carbonate diagenesis. *Sedimentology* **42**, 805–824.

Bertram M. A., Mackenzie F. T., Bishop F. C. and Bischoff W. D. (1991) Influence of temperature on the stability of magnesian calcite. *Am. Miner.* **76**, 1889–1896.

Bischoff W. D., Bertram M. A., Mackenzie F. T. and Bishop F. C. (1993) Diagenetic stabilization pathways of magnesian calcites. *Carbonates Evap.* **81**, 82–89.

Blättler C. L., Miller N. R. and Higgins J. A. (2015) Mg and Ca isotope signatures of authigenic dolomite in siliceous deep-sea sediments. *Earth Planet. Sci. Lett.* **419**, 32–42.

Buhl D., Immenhauser A., Smeulders G., Kabiri L. and Richter D. K. (2007) Time series δ^{26}Mg analysis in speleothem calcite: kinetic versus equilibrium fractionation, comparison with other proxies and implications for palaeoclimate research. *Chem. Geol.* **244**, 715–729.

Cao C., Wang W., Liu L., Shen S. and Summons R. E. (2008) Two episodes of ^{13}C-depletion in organic carbon in the latest Permian: evidence from the terrestrial sequences in northern Xinjiang, China. *Earth Planet. Sci. Lett.* **270**, 251–257.

Carpenter A. B. (1980) The chemistry of dolomite formation I: the stability of dolomite. In *Concepts and Models of Dolomitization*, vol. 28 (eds. D. H. Zenger, J. B. Dunham and R. L. Ethington). Society of Economic Paleontologists and Mineralogists. Special Publication, pp. 111–121.

Chang V. T. C., Williams R. J. P., Makishima A., Belshawl N. S. and O'Nions R. K. (2004) Mg and Ca isotope fractionation during $CaCO_3$ biomineralisation. *Biochem. Biophys. Res. Commun.* **323**, 79–85.

Cole D. R. and Chakraborty S. (2001) Rates and mechanisms of isotopic exchange. *Rev. Mineral. Geochem.* **43**, 83–223.

Davies G. R. and Smith L. B. (2006) Structurally controlled hydrothermal dolomite reservoir facies: an overview. *AAPG Bull.* **90**, 1641–1690.

Dickson J. A. D. (1966) Carbonate identification and genesis as revealed by staining. *J. Sediment. Res.* **36**, 494–505.

Dickson J. A. D., Montanez I. P. and Saller A. H. (2001) Hypersaline burial diagenesis delineated by component isotopic analysis, late Paleozoic limestones, West Texas. *J. Sediment. Res.* **71**, 372–379.

Dong A., Zhu X.-K., Li S.-Z., Kendall B., Wang Y. and Gao Z. (2016) Genesis of a giant Paleoproterozoic strata-bound magnesite deposit: constraints from Mg isotopes. *Precambr. Res.* **281**, 673–683.

Elderfield H. (1986) Strontium isotope stratigraphy. *Paleogeogr. Paleoclimatol. Paleoecol.* **57**, 71–90.

Elderfield H. and Gieskes J. M. (1982) Sr isotopes in interstitial waters of marine sediments from Deep Sea Drilling Project cores. *Nature* **300**, 493–497.

Fantle M. S. and Higgins J. (2014) The effects of diagenesis and dolomitization on Ca and Mg isotopes in marine platform carbonates: implications for the geochemical cycles of Ca and Mg. *Geochim. Cosmochim. Acta* **142**, 458–481.

Friedman G. M. (1965) Occurrence and stability relationships of aragonite, high-magnesian calcite, and low-magnesian calcite under deep-sea conditions. *Geol. Soc. Am. Bull.* **76**, 1191–1196.

Galy A., Bar-Matthews M., Halicz L. and O'Nions R. K. (2002) Mg isotopic composition of carbonate: insight from speleothem formation. *Earth Planet. Sci. Lett.* **201**, 105–115.

Galy A., Yoffe O., Janney P. E., Williams R. W., Cloquet C., Alard O., Halicz L., Wadhwa M., Hutcheon I. D., Ramon E. and Carignan J. (2003) Magnesium isotope heterogeneity of the isotopic standard SRM980 and new reference materials for magnesium-isotope-ratio measurements. *J. Anal. At. Spectrom.* **18**, 1352–1356.

Gao T., Ke S., Teng F.-Z., Chen S., He Y. and Li S.-G. (2016) Magnesium isotope fractionation during dolostone weathering. *Chem. Geol.* **445**, 14–23.

Gasparrini M., Bechstädt T. and Boni M. (2006) Massive hydrothermal dolomites in the southwestern Cantabrian Zone (Spain) and their relation to the Late Variscan evolution. *Mar. Petrol. Geol.* **23**, 543–568.

Geske A., Zorlu J., Richter D. K., Buhl D., Niedermayr A. and Immenhauser A. (2012) Impact of diagenesis and low grade metamorphosis on isotope (δ^{26}Mg, δ^{13}C, δ^{18}O and ^{87}Sr/^{86}Sr) and elemental (Ca, Mg, Mn, Fe and Sr) signatures of Triassic sabkha dolomites. *Chem. Geol.* **332–333**, 45–64.

Geske A., Goldstein R. H., Mavromatis V., Richter D. K., Buhl D., Kluge T., John C. M. and Immenhauser A. (2015a) The magnesium isotope (δ^{26}Mg) signature of dolomites. *Geochim. Cosmochim. Acta* **149**, 131–151.

Geske A., Lokier S., Dietzel M., Richter D. K., Buhl D. and Immenhauser A. (2015b) Magnesium isotope composition of Sabkha porewater and related (sub-)recent stoichiometric dolomites, Abu Dhabi (UAE). *Chem. Geol.* **393–394**, 112–124.

Graf D. L. and Goldsmith J. R. (1956) Some hydrothermal syntheses of dolomite and protodolomite. *J. Geol.* **64**, 173–186.

Haas J., Budai T., Győri O., Kele S. and Lokier S. (2014) Multiphase partial and selective dolomitization of Carnian reef limestone (Transdanubian Range, Hungary). *Sedimentology* **61**, 836–859.

He W., Tang T., Yue M., Deng J., Pan G., Xing G., Luo M., Xu Y., Wei Y., Zhang Z., Xiao Y. and Zhang K. (2014) Sedimentary and tectonic evolution of Nanhuan-Permian in South China. *Earth Sci. (J. China Univ. Geosci.)* **39**, 929–953 (in Chinese with English abstract).

Higgins J. A. and Schrag D. P. (2010) Constraining magnesium cycling in marine sediments using magnesium isotopes. *Geochim. Cosmochim. Acta* **74**, 5039–5053.

Higgins J. A. and Schrag D. P. (2015) The Mg isotopic composition of Cenozoic seawater – evidence for a link between Mg-clays, seawater Mg/Ca, and climate. *Earth Planet. Sci. Lett.* **416**, 73–81.

Hippler D., Buhl D., Witbaard R., Richter D. K. and Immenhauser A. (2009) Towards a better understanding of magnesium-isotope ratios from marine skeletal carbonates. *Geochim. Cosmochim. Acta* **73**, 6134–6146.

Hodgson W. A. (1966) Carbon and oxygen isotope ratios in diagenetic carbonates from marine sediments. *Geochim. Cosmochim. Acta* **30**, 1223–1233.

Hua C. (2014) Evaluation on oil and gas geological conditions of upper marine formation assemblage in Jurong area of Lower Yangtze area. *Jiangsu Geology* **38**, 200–205 (in Chinese with English abstract).

Huang K.-J., Shen B., Lang X.-G., Tang W.-B., Peng Y., Ke S., Kaufman A. J., Mao H.-R. and Li F.-B. (2015) Magnesium isotopic compositions of the Mesoproterozoic dolostones: implications for Mg isotopic systematics of marine carbonates. *Geochim. Cosmochim. Acta* **164**, 333–351.

Huang Y., Zhao S., Yang R. and Xiao Z. (2014) Study on accumulation characteristics by hydrocarbon inclusions in Huangqiao and Jurong area with the context of polycyclic sedimentation. *J. Yanan Univ. (Nat. Sci. Ed.)* **33**, 41–45 (in Chinese with English abstract).

Immenhauser A., Buhl D., Richter D., Niedermayr A., Riechelmann D., Dietzel M. and Schulte U. (2010) Magnesium-isotope fractionation during low-Mg calcite precipitation in a limestone cave – field study and experiments. *Geochim. Cosmochim. Acta* **74**, 4346–4364.

Jacobson A. D., Zhang Z., Lundstrom C. and Huang F. (2010) Behavior of Mg isotopes during dedolomitization in the Madison Aquifer, South Dakota. *Earth Planet. Sci. Lett.* **297**, 446–452.

Jin Z. (2006) A study on the distribution of saline-deposit in southern china. *Oil Gas Geol.* **27**, 571–583 (in Chinese with English abstract).

Kasemann S. A., Pogge von Strandmann P. A. E., Prave A. R., Fallick A. E., Elliott T. and Hoffmann K.-H. (2014) Continental weathering following a Cryogenian glaciation: evidence from calcium and magnesium isotopes. *Earth Planet. Sci. Lett.* **396**, 66–77.

Katz A. and Matthews A. (1977) The dolomitization of $CaCO_3$: an experimental study at 252–295 °C. *Geochim. Cosmochim. Acta* **41**, 297–308.

Kırmacı M. Z. and Akdağ K. (2005) Origin of dolomite in the Late Cretaceous-Paleocene limestone turbidites, Eastern Pontides, Turkey. *Sediment. Geol.* **181**, 39–57.

Kırmacı M. Z. (2008) Dolomitization of the late Cretaceous-Paleocene platform carbonates, Gölköy (Ordu), eastern Pontides, NE Turkey. *Sediment. Geol.* **203**, 289–306.

Kolchugin A. N., Immenhauser A., Walter B. F. and Morozov V. P. (2016) Diagenesis of the palaeo-oil-water transition zone in a Lower Pennsylvanian carbonate reservoir: constraints from cathodoluminescence microscopy, microthermometry, and isotope geochemistry. *Mar. Petrol. Geol.* **72**, 45–61.

Korte C., Kozur H. W., Bruckschen P. and Veizer J. (2003) Strontium isotope evolution of Late Permian and Triassic seawater. *Geochim. Cosmochim. Acta* **67**, 47–62.

Korte C., Kozur H. W. and Veizer J. (2005) $\delta^{13}C$ and $\delta^{18}O$ values of Triassic brachiopods and carbonate rocks as proxies for coeval seawater and palaeotemperature. *Paleogeogr. Paleoclimatol. Paleoecol.* **226**, 287–306.

Lapponi F., Bechstädt T., Boni M., Banks D. A. and Schneider J. (2014) Hydrothermal dolomitization in a complex geodynamic setting (Lower Palaeozoic, northern Spain). *Sedimentology* **61**, 411–443.

Lavoie D., Jackson S. and Girard I. (2014) Magnesium isotopes in high-temperature saddle dolomite cements in the lower Paleozoic of Canada. *Sediment. Geol.* **305**, 58–68.

Li F.-B., Teng F.-Z., Chen J.-T., Huang K.-J., Wang S.-J., Ma H.-R., Peng Y.-B. and Shen B. (2016a) Constraining ribbon rock dolomitization by Mg isotopes: implications for the 'dolomite problem'. *Chem. Geol.* **445**, 208–220.

Li W., Beard B. L. and Johnson C. M. (2011) Exchange and fractionation of Mg isotopes between epsomite and saturated $MgSO_4$ solution. *Geochim. Cosmochim. Acta* **75**, 1814–1828.

Li W., Chakraborty S., Beard B. L., Romanek C. S. and Johnson C. M. (2012) Magnesium isotope fractionation during precipitation of inorganic calcite under laboratory conditions. *Earth Planet. Sci. Lett.* **333–334**, 304–316.

Li W., Beard B. L., Li C. and Johnson C. M. (2014) Magnesium isotope fractionation between brucite $[Mg(OH)_2]$ and Mg aqueous species: implications for silicate weathering and biogeochemical processes. *Earth Planet. Sci. Lett.* **394**, 82–93.

Li W., Beard B. L., Li C., Xu H. and Johnson C. M. (2015) Experimental calibration of Mg isotope fractionation between dolomite and aqueous solution and its geological implications. *Geochim. Cosmochim. Acta* **157**, 164–181.

Li W., Beard B. L. and Li S. (2016b) Precise measurement of stable potassium isotope ratios using a single focusing collision cell multi-collector ICP-MS. *J. Anal. At. Spectrom.* **31**, 1023–1029.

Ling M.-X., Sedaghatpour F., Teng F.-Z., Hays P. D., Strauss J. and Sun W. (2011) Homogeneous magnesium isotopic composition of seawater: an excellent geostandard for Mg isotope analysis. *Rapid Commun. Mass Spectrom.* **25**, 2828–2836.

Ling H.-F., Feng H.-Z., Pan J.-R., Jiang S.-Y., Chen Y.-Q. and Chen X. (2007) Carbon isotope variation through the Neoproterozoic Doushantuo and Dengying Formations, South China: implications for chemostratigraphy and paleoenvironmental change. *Paleogeogr. Paleoclimatol. Paleoecol.* **254**, 158–174.

Liu C., Wang Z., Raub T. D., Macdonald F. A. and Evans D. A. D. (2014) Neoproterozoic cap-dolostone deposition in stratified glacial meltwater plume. *Earth Planet. Sci. Lett.* **404**, 22–32.

Liu D., Gong S., Liu D., Ceng Q., Xiao X., Tian H., Shen G. and Li X. (2005) Investigation on the phases of organic inclusion from Gourong-Huangqiao region, Jiangsu province, and its trapped temperature and pressure calculated by pvtsim modeling. *Acta Petrol. Sin.* **21**, 1435–1448 (in Chinese with English abstract).

Machel H. G. and Anderson J. H. (1989) Pervasive subsurface dolomitization of the Nisku Formation in central Alberta. *J. Sediment. Res.* **59**, 891–911.

Mathieu J., Kontak D. J., Turner E. C., Fayek M. and Layne G. (2015) Geochemistry of Phanerozoic diagenesis on Victoria Island, NWT, Canada. *Chem. Geol.* **415**, 47–69.

Mavromatis V., Gautier Q., Bosc O. and Schott J. (2013) Kinetics of Mg partition and Mg stable isotope fractionation during its incorporation in calcite. *Geochim. Cosmochim. Acta* **114**, 188–203.

Mavromatis V., Meister P. and Oelkers E. H. (2014) Using stable Mg isotopes to distinguish dolomite formation mechanisms: a case study from the Peru Margin. *Chem. Geol.* **385**, 84–91.

McCormack J. M., Bahr A., Gerdes A., Tütken T. and Prinz-Grimm P. (2015) Preservation of successive diagenetic stages in Middle Triassic bonebeds: evidence from in situ trace element and strontium isotope analysis of vertebrate fossils. *Chem. Geol.* **410**, 108–123.

McHargue T. R. and Price R. C. (1982) Dolomite from clay in argillaceous or shale-associated marine carbonates. *J. Sediment. Res.* **52**, 873–886.

Molony B. and Ridge M. J. (1968) Kinetics of the dehydration of calcium sulphate dihydrate in vacuo. *Aust. J. Chem.* **21**, 1063–1065.

Ovtcharova M., Goudemand N., Hammer Ø., Guodun K., Cordey F., Galfetti T., Schaltegger U. and Bucher H. (2015) Developing a strategy for accurate definition of a geological boundary through radio-isotopic and biochronological dating: the Early-Middle Triassic boundary (South China). *Earth-Sci. Rev.* **146**, 65–76.

Pearce C. R., Saldi G. D., Schott J. and Oelkers E. H. (2012) Isotopic fractionation during congruent dissolution, precipitation and at equilibrium: evidence from Mg isotopes. *Geochim. Cosmochim. Acta* **92**, 170–183.

Peng Y., Shen B., Lang X.-G., Huang K.-J., Chen J.-T., Yan Z., Tang W.-B., Ke S., Mao H.-R. and Li F.-B. (2016) Constraining dolomitization by Mg isotopes: a case study from partially dolomitized limestones of the middle Cambrian Xuzhuang Formation, North China. *Geochem. Geophys. Geosyst.* **17**, 1109–1129.

Pinilla C., Blanchard M., Balan E., Natarajan S. K., Vuilleumier R. and Mauri F. (2015) Equilibrium magnesium isotope fractionation between aqueous Mg^{2+} and carbonate minerals: insights from path integral molecular dynamics. *Geochim. Cosmochim. Acta* **163**, 126–139.

Pogge von Strandmann P. A. E. (2008) Precise magnesium isotope measurements in core top planktic and benthic foraminifera. *Geochem. Geophys. Geosyst.* **9**.

Pogge von Strandmann P. A. E., Forshaw J. and Schmidt D. N. (2014) Modern and Cenozoic records of seawater magnesium from foraminiferal Mg isotopes. *Biogeosciences* **11**, 5155–5168.

Qing H., Bosence D. W. J. and Rose E. P. E. (2001) Dolomitization by penesaline sea water in Early Jurassic peritidal platform carbonates, Gibraltar, western Mediterranean. *Sedimentology* **48**, 153–163.

Rameil N. (2008) Early diagenetic dolomitization and dedolomitization of Late Jurassic and earliest Cretaceous platform carbonates: a case study from the Jura Mountains (NW Switzerland, E France). *Sediment. Geol.* **212**, 70–85.

Riechelmann S., Buhl D., Schröder-Ritzrau A., Spötl C., Riechelmann D. F. C., Richter D. K., Kluge T., Marx T. and Immenhauser A. (2012) Hydrogeochemistry and fractionation pathways of Mg isotopes in a continental weathering system: lessons from field experiments. *Chem. Geol.* **300–301**, 109–122.

Riechelmann S., Mavromatis V., Buhl D., Dietzel M., Eisenhauer A. and Immenhauser A. (2016) Impact of diagenetic alteration on brachiopod shell magnesium isotope (δ^{26}Mg) signatures: experimental versus field data. *Chem. Geol.* **440**, 191–206.

Rollion-Bard C., Saulnier S., Vigier N., Schumacher A., Chaussidon M. and Lécuyer C. (2016) Variability in magnesium, carbon and oxygen isotope compositions of brachiopod shells: implications for paleoceanographic studies. *Chem. Geol.* **423**, 49–60.

Ronchi P., Jadoul F., Ceriani A., Di Giulio A., Scotti P., Ortenzi A. and Previde Massara E. (2011) Multistage dolomitization and distribution of dolomitized bodies in Early Jurassic carbonate platforms (Southern Alps, Italy). *Sedimentology* **58**, 532–565.

Rosenberg P. E. and Holland H. D. (1964) Calcite-dolomite-magnesite stability relations in solutions at elevated temperatures. *Science* **145**, 700–701.

Rudnick R. L. and Gao S. (2003) 3.01–Composition of the continental crust. In *Treatise on Geochemistry* (eds. H. D. Holland and K. K. Turekian), first ed. Pergamon, Oxford, pp. 1–64.

Rustad J. R., Casey W. H., Yin Q.-Z., Bylaska E. J., Felmy A. R., Bogatko S. A., Jackson V. E. and Dixon D. A. (2010) Isotopic fractionation of Mg^{2+}(aq), Ca^{2+}(aq), and Fe^{2+}(aq) with carbonate minerals. *Geochim. Cosmochim. Acta* **74**, 6301–6323.

Saenger C. and Wang Z. (2014) Magnesium isotope fractionation in biogenic and abiogenic carbonates: implications for paleoenvironmental proxies. *Quat. Sci. Rev.* **90**, 1–21.

Saulnier S., Rollion-Bard C., Vigier N. and Chaussidon M. (2012) Mg isotope fractionation during calcite precipitation: an experimental study. *Geochim. Cosmochim. Acta* **91**, 75–91.

Schauble E. A. (2011) First-principles estimates of equilibrium magnesium isotope fractionation in silicate, oxide, carbonate and hexaaquamagnesium(2+) crystals. *Geochim. Cosmochim. Acta* **75**, 844–869.

Shen B., Dong L., Xiao S., Lang X., Huang K., Peng Y., Zhou C., Ke S. and Liu P. (2016) Molar tooth carbonates and benthic methane fluxes in Proterozoic oceans. *Nat. Commun.* **7**, 10317.

Shu L., Zhou X., Deng P., Yu X., Wang B. and Zu F. (2004) Geological features and tectonic evolution of Meso-Cenozoic basins in southeastern China. *Reg. Geol. China* **23**, 876–884 (in Chinese with English abstract).

Song H., Wignall P. B., Tong J., Song H., Chen J., Chu D., Tian L., Luo M., Zong K., Chen Y., Lai X., Zhang K. and Wang H. (2015) Integrated Sr isotope variations and global environmental changes through the Late Permian to early Late Triassic. *Earth Planet. Sci. Lett.* **424**, 140–147.

Sun S. Q. (1994) A reappraisal of dolomite abundance and occurrence in the Phanerozoic: perspective. *J. Sediment. Res.* **64**, 396–404.

Teng F.-Z., Li W.-Y., Ke S., Marty B., Dauphas N., Wu F.-Y. and Pourmand A. (2010) Magnesium isotopic composition of the Earth and chondrites. *Geochim. Cosmochim. Acta* **74**, 4150–4166.

Teng F.-Z., Li W.-Y., Ke S., Yang W., Liu S.-A., Sedaghatpour F., Wang S.-J., Huang K.-J., Hu Y., Ling M.-X., Xiao Y., Liu X.-M., Li X.-W., Gu H.-O., Sio C. K., Wallace D. A., Su B.-X., Zhao L., Chamberlin J., Harrington M. and Brewer A. (2015) Magnesium isotopic compositions of international geological reference materials. *Geostand. Geoanal. Res.* **39**, 329–339.

Teng F.-Z. (2017) Magnesium isotope geochemistry. *Rev. Mineral. Geochem.* **82**, 219–287.

Teng F.-Z., Dauphas N. and Watkins J. M. (2017) Non-traditional stable isotopes: retrospective and prospective. *Rev. Mineral. Geochem.* **82**, 1–26.

Tipper E., Galy A., Gaillardet J., Bickle M., Elderfield H. and Carder E. (2006) The magnesium isotope budget of the modern ocean: constraints from riverine magnesium isotope ratios. *Earth Planet. Sci. Lett.* **250**, 241–253.

Tong J. and Yin H. (1997) The marine Triassic sequence stratigraphy of Lower Yangtze. *Science in China* **27**, 407–411 (in Chinese).

Urey H. C. (1947) The thermodynamic properties of isotopic substances. *J. Chem. Soc.* **5**, 562–581.

Vakhlu V., Bassi P. S. and Mehta S. K. (1985) Thermoanalytical studies on gypsum dehydration. *Trans. Indian Ceram. Soc.* **44**, 29–32.

Veizer J., Ala D., Azmy K., Bruckschen P., Buhl D., Bruhn F., Carden G. A. F., Diener A., Ebneth S., Godderis Y., Jasper T., Korte C., Pawellek F., Podlaha O. G. and Strauss H. (1999) $^{87}Sr/^{86}Sr$, $\delta^{13}C$ and $\delta^{18}O$ evolution of Phanerozoic seawater. *Chem. Geol.* **161**, 59–88.

Walter B. F., Immenhauser A., Geske A. and Markl G. (2015) Exploration of hydrothermal carbonate magnesium isotope signatures as tracers for continental fluid aquifers, Schwarzwald mining district, SW Germany. *Chem. Geol.* **400**, 87–105.

Wang L., Hu W., Wang X., Cao J. and Chen Q. (2014) Seawater normalized REE patterns of dolomites in Geshan and Panlongdong sections, China: implications for tracing dolomitization and diagenetic fluids. *Mar. Petrol. Geol.* **56**, 63–73.

Wang Z., Hu P., Gaetani G., Liu C., Saenger C., Cohen A. and Hart S. (2013) Experimental calibration of Mg isotope fractionation between aragonite and seawater. *Geochim. Cosmochim. Acta* **102**, 113–123.

Wilkinson B. H. and Algeo T. J. (1989) Sedimentary carbonate record of calcium-magnesium cycling. *Am. J. Sci.* **289**, 1158–1194.

Wombacher F., Eisenhauer A., Böhm F., Gussone N., Regenberg M., Dullo W. C. and Rüggeberg A. (2011) Magnesium stable isotope fractionation in marine biogenic calcite and aragonite. *Geochim. Cosmochim. Acta* **75**, 5797–5818.

Young E. D. and Galy A. (2004) The isotope geochemistry and cosmochemistry of magnesium. *Rev. Mineral. Geochem.* **55**, 197–230.

Young E. D., Manning C. E., Schauble E. A., Shahar A., Macris C. A., Lazar C. and Jordan M. (2015) High-temperature equilibrium isotope fractionation of non-traditional stable isotopes: experiments, theory, and applications. *Chem. Geol.* **395**, 176–195.

Zevin L. S. (1977) A method of quantitative phase analysis without standards. *J. Appl. Crystallogr.* **10**, 147–150.

Zhang F., Xu H., Konishi H. and Roden E. E. (2010) A relationship between d_{104} value and composition in the calcite-disordered dolomite solid-solution series. *Am. Miner.* **95**, 1650–1656.

Associate editor: Andrew D. Jacobson